Journal of Power Sources 565 (2023) 232911

Contents lists available at ScienceDirect

Journal of Power Sources

journal homepage: www.elsevier.com/locate/jpowsour

Impact of pore-forming by PSF in the anode on power generation and mass transport characteristics of direct formic acid fuel cell

Madihah Miskan [a], Mototake Furuhashi [b], Yugo Osaka [c], Akio Kodama [d], Takuya Tsujiguchi [c,*]

[a] Division of Mechanical Engineering, Graduate School of Natural Science and Technology, Kanazawa University, Kanazawa, Japan
[b] Advanced Development Research Department, JTEKT Corporation, Japan
[c] Faculty of Mechanical Engineering, Institute of Science and Engineering, Kanazawa University, Kanazawa, Japan
[d] Institute for Frontier Science Initiative, Kanazawa University, Kanazawa, Japan

HIGHLIGHTS

- A pore-designed anode catalyst layer for DFAFC is fabricated using pore former.
- Electrospinning is used to prepare polystyrene fiber (PSF) as pore former.
- Power density and mass transport rate can be improved by pore forming.
- Optimal diameter and amount of PSF are found showing high DFAFC power density.

ARTICLE INFO

Keywords:
Direct formic acid fuel cell
Pore structure of catalyst layer
Two-phase mass transport
Crossover flux
Pore former
Electrospinning
Polystyrene fiber

ABSTRACT

Controlling the mass transport in the anode plays a crucial role in the higher performance of direct formic acid fuel cells (DFAFCs) due to the two-phase flow of the liquid fuel reactant with the CO_2 gaseous product. A pore-designed anode catalyst layer using polystyrene fiber (PSF) as a pore former is fabricated to investigate the relationship between the pore properties of the DFAFC and power generation/mass transport characteristics by controlling the diameters and amounts of the PSF. PSFs with various average diameters are prepared by the electrospinning. The anode catalyst containing the PSFs is coated by spraying method on the membrane. The PSFs in the anode catalyst layer are removed by soaking in ethyl acetate, resulting the pore forming in the catalyst layer. DFAFC using 3 μm-0.5 PSF as pore former shows the highest crossover flux at the operating temperatures of 30 °C and 60 °C, which results in 25% and 5% increases of the maximum power density respectively, as compared to without-PSF. This indicates that the appropriate PSF properties, i.e., diameter and amount, can contribute to enhancing the liquid saturation in the catalyst layer by increasing the fuel transport and CO_2 removal, resulting in a performance improvement.

1. Introduction

Hydrogen-fed polymer electrolyte membrane fuel cells (PEMFCs) are recognized as a pioneering type of fuel cell that excels in a variety of application including the automotive industry. However, because hydrogen is a highly flammable gas, its delivery and storage pose challenges that must be addressed with caution [1]. Direct liquid fuel cells (DLFCs), on the other hand, have advantages in terms of safe fuel storage and are more practical, thus leading to their rapidly growing interest in portable electronic device applications [2].

One of the several types of DLFCs, the direct formic acid fuel cell (DFAFC), has gained attention due to its fast electro-oxidation in the anode and ability to achieve a higher power density than the direct methanol fuel cell (DMFC) [3–5]. Moreover, its lower formic acid crossover flux (CF) rate has also enabled it to operate with a thinner electrolyte membrane and higher fuel concentrations [2,6]. The DFAFC typically consists of anode and cathode electrodes, each of which comprises a catalyst layer and a diffusion layer and is separated by a proton exchange membrane. It generates electricity when the fuel reaches the anode catalyst layer and is oxidized, producing CO_2, protons, and electrons. The generated protons will then transfer through the polymer electrolyte membrane to the cathode, while electrons will pass through

* Corresponding author.
E-mail address: tsujiguchi@se.kanazawa-u.ac.jp (T. Tsujiguchi).

https://doi.org/10.1016/j.jpowsour.2023.232911
Received 6 January 2023; Received in revised form 18 February 2023; Accepted 1 March 2023
Available online 7 March 2023

the external circuit to generate electricity. In the presence of protons and electrons from the anode, O_2 is reduced in the cathode to produce H_2O.

Because the DLFC employs a liquid as a reactant, it has been identified that during cell operation, a two-phase counter flow of the liquid fuel reactant with the CO_2 gaseous product exists in the anode electrode and becomes a critical issue for the higher efficiency of the DLFC performance [7–9]. This is because the removal of the CO_2 gaseous product from the anode catalyst layer is required to maintain the good dispersion of the liquid fuel towards the anode catalyst layer [8–12]. In addition, when the rate of CO_2 gaseous removal is less than the rate of its production, the CO_2 gaseous accumulates in the porous electrodes (diffusion layer and catalyst layer) and limits the liquid fuel transport to the anode catalyst layer which causes a sluggish electro-oxidation reaction. Therefore, several strategies have been carried out since then in an attempt to mitigate the mass transport limitation issue of the DLFC anode electrode. This includes research of improving the anode flow field design [13,14], as well as in the anode diffusion layer [15–18]. Despite the focus of research in these two areas, the anode catalyst layer is also an important area because the electro-oxidation reaction occurs for the cell power generation.

Few studies have reported that modifying the anode catalyst layer to account for pore structure enhancement through the use of a pore forming agent has improved the mass transport balance in the anode electrode [19–23]. Tucker et al. [19] reported that by introducing 50% Li_2CO_3 particle as a pore forming agent in the DMFC anode catalyst layer, which was then removed by soaking it in H_2SO_4, they were able to achieve a more open pore structure in the catalyst layer. They also stated that the decrease in the concentration overpotential observed in the polarization curve is due to the increased mass transport caused by increasing the pore size. However, particle size optimization is still necessary to achieve the optimal size for the maximum cell performance. In another DMFC study, Liu et al. [20] used a dual-layer catalytic anode with different porosities with the inner layer being less porous than the outer layer to improve the methanol permeation resistance through the membrane. To create the porous outer layer, NH_4HCO_3 particles were used which resulted in a 40% performance improvement for their 30 °C cell operating temperature. Bauskar et al. [21] discovered the optimal amount of the pore forming agent in the DFAFC study by varying two different amounts of Li_2CO_3 (17.5% and 50%) particles on their anode catalyst layer for the improvement of the formic acid transport. They also stated that the increased mass transport had no effect on the formic acid CF, but no experimental details related to the fuel transport were provided in their study. Later, in another DMFC study, Lee et al. [22] optimized the different particle sizes of the SiO_2 pore forming agent. It was discovered that larger pores provided a better performance than the smaller pores due to their ability to easily convey fuel to the catalyst particle, which caused improvement in the activation loss, leading to an enhanced cell performance. Huang et al. [23] found that the combination of the pore structure improvement of the anode catalyst layer along with a microporous layer prepared by adding the MgO sacrificial pore former had greatly enhanced the DMFC performance due to better catalyst utilization demonstrated by the CV measurements. Although some of these studies have demonstrated that pore properties, such as the pore diameters, amounts and/or shape, have a significant impact on the DLFC performance, the relationship between the pore properties and the CF, which defines the quantitative rate of mass transport, has not been reported, particularly for the DFAFC. In this context, the effect of the pore properties in the anode catalyst layer created by the pore former on the DFAFC power generation characteristics and formic acid fuel CF were investigated in this study. In order to control the shape, size, and amount of the pore, polystyrene fibers (PSFs) having different diameters were prepared as pore formers by electrospinning. In contrast to the previously mentioned particle pore former, which can only control its diameter, the fiber has the advantage that it can easily be obtained by electrospinning, which can control both the diameter and the length.

Electrospinning has been widely used as a promising technique to fabricate micro- and nanofibers, which provides excellent control over the properties of the fiber formed, such as the fiber diameters, that are derived from various polymer solutions under a very high electrical field [24]. In the present study, by using polystyrene (PS) as a polymer solution, which has been chosen due to its characteristic of being easily removed via chemical treatment [25], as well as the fact that it is classified as a polymer compound that is suitable to form a fiber using electrospinning [24], we fabricated PSF with different diameters using an electrospinning technique [26,27], which is the first to be used as a pore forming agent for modification of the anode catalyst layer's porous structure. The power generation characteristics and crossover flux of the DFAFC was investigated at different operating temperatures (30 °C and 60 °C) and formic acid concentrations (3 M, 5 M and 7 M) by using several anodes prepared with different diameters of the PSF (1-μm, 3-μm and 5-μm) containing different amounts of PSF (0.3 and 0.5) in order to discuss the relationship of the pore properties to the power generation and the mass transport characteristics.

2. Experimental methods

2.1. Fabrication of pore-designed anode catalyst layer

2.1.1. Fabrication of PSF by electrospinning

Electrospun PSF with different diameters of 1-μm, 3-μm and 5-μm were fabricated by electrospinning (Nanon-01B, MECC Co., Ltd.). The PS polymer (Mw ~ 280,000, Sigma) was used, and a PS solution was prepared by dissolving the PS into a solvent mixture containing N,N-dimethylformamide (DMF) and tetrahydrofuran (THF) in the weight ratio of 50:50. By using different concentrations of the PS solution and different electrospinning operating conditions, the different diameters of the PSF were obtained [26,27]. To obtain a PSF of 3-μm and 5-μm average diameters, a 23 wt% PS solution was used, while the 0.025 wt% tetrabutylammonium bromide (TBAB) salt was added to a 20 wt% concentration of the PS solution to obtain the 1-μm diameter PSF. All of the PS solutions were then stirred for 6 h at room temperature using a mechanical stirrer to achieve a homogeneous solution.

The homogeneous PS solutions were then transferred to a syringe equipped with a tube and a needle tip. For the electrospinning, the syringe was horizontally clamped on the syringe pump. A grounded cylinder collector was covered with aluminum foil for the collection of the PSF, and was rotated at 100 rpm with the tip-to-collector distance varying from 15 to 20 cm. The flow rates and the voltage of the electrospinning were varied from 0.5 to 2 mL/h and 15 to 30 kV, respectively, to obtain 1-μm, 3-μm and 5-μm diameter PSFs. The diameters were confirmed by scanning electron microscopy (SEM, SU1510 Hitachi).

2.1.2. Controlling the length of PSF

The PSFs were then shortened to a similar average length that was controlled by using an ultrasonic homogenizer (Sonifier SFX250, Branson). The electrospun PSF was weighed in two different weight ratios, i.e., weight of PSF to the carbon of Pd/C, which is used as the anode catalyst, of 30:70 and 50:50, before being placed in a 50-mL beaker containing isopropyl alcohol as the homogenizing medium. It was then homogenized in the ultrasonic homogenizer. The homogenizing time was varied from 15 to 40 min while the power output was varied from 20% to 70% to achieve an average PSF length of 5 to 20 μm for all the PSF diameters (1-μm, 3-μm and 5-μm). The shortened PSFs for all the diameters of the PSF were then observed by using SEM.

2.1.3. Catalyst coated membrane (CCM) preparation using PSF as a pore former to form a pore-designed anode catalyst layer

The anode catalyst ink was prepared by mixing the Pd/C catalyst (40 wt% Pd, Ishifuku Metal Industry Co., Ltd.) with deionized water and a 5 wt% of Nafion solution (Wako Pure Chemical Industries, Ltd.). The

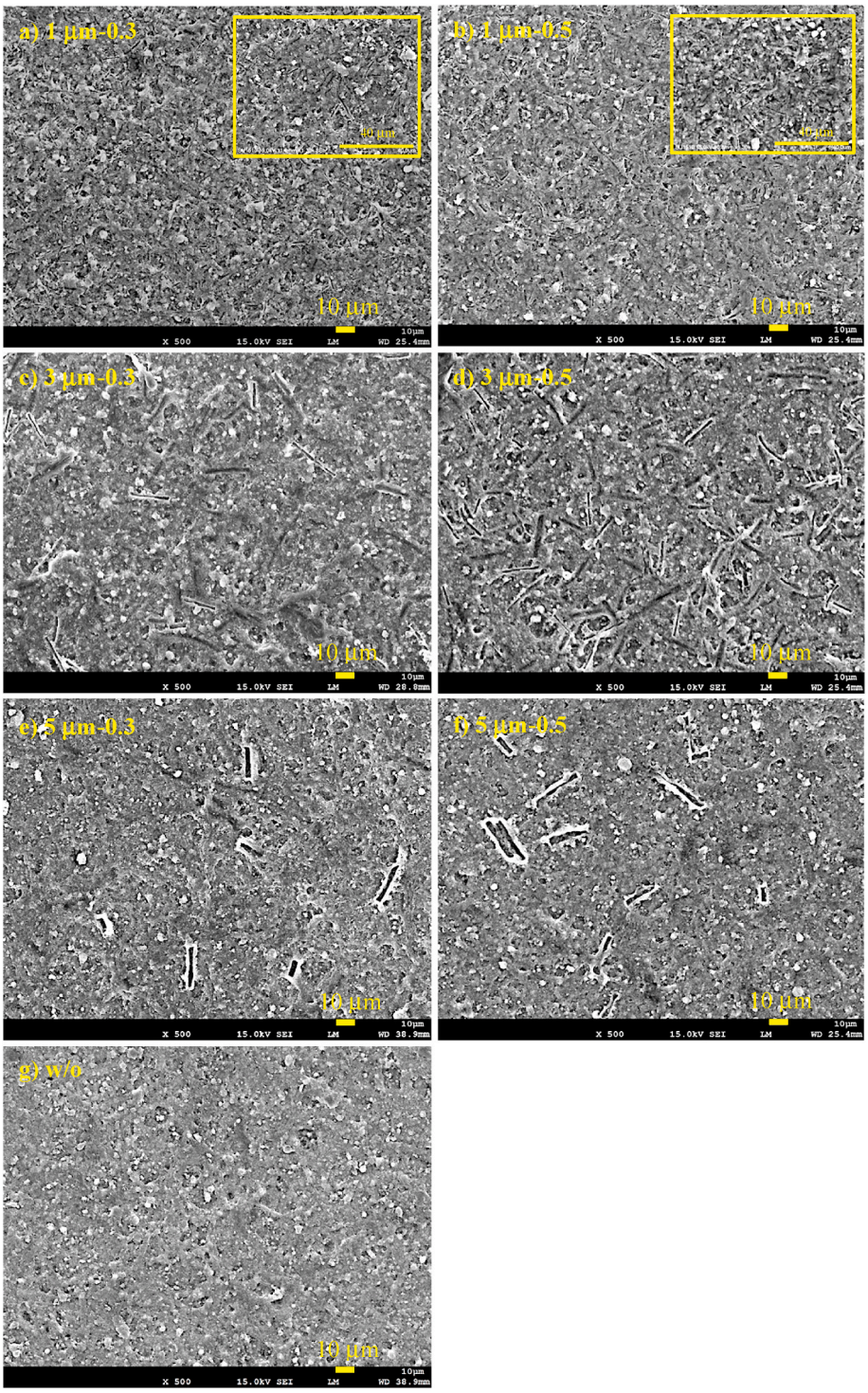

Fig. 1. Morphological images of the pore-designed anode catalyst layers of; a) 1 μm-0.3, b) 1 μm-0.5, c) 3 μm-0.3, d) 3 μm-0.5, e) 5 μm-0.3, f) 5 μm-0.5 and g) without-PSF.

previously shortened PSF, which is in the isopropyl alcohol, was then added to the anode catalyst ink and homogenized in an ultrasonic bath (W-113A, Honda Electronics, Co., Ltd.) for 13 min. The homogenized catalyst ink was then sprayed (ExactaCoat, SONO-TEK) on the membrane (Nafion 212) with an active area of 5.29 cm^2 (2.3 cm × 2.3 cm) forming a 1.2–1.4 mg-Pd/cm^2 loading. The loading of the Nafion ionomer was controlled by the proportion of I/C, i.e., the weight ratio of ionomer and carbon was 1.0.

For the cathode electrode, Pt/C (46.5 wt% of Pt, TEC10E50E, Tanaka Holdings Co., Ltd.) was used as the catalyst and mixed with the same components as the anode, but without the pore forming agent (PSF). The cathode catalyst ink was then sprayed on the other side of the membrane containing the anode catalyst layer to form a CCM. To avoid flooding, a hydrophobic microporous layer (MPL) was then coated on the cathode catalyst layer by spraying, with the composition of carbon black (Vulcan XC-72R, Fuel Cell Store), deionized water, isopropyl alcohol, and 12 wt % PTFE dispersion to achieve a 0.3 mg-C/cm^2 carbon loading.

In order to form pores, the PSF was removed from the anode catalyst

layer by soaking the CCM in ethyl acetate for 2 h. The excessive ethyl acetate was then removed by putting the CCM in 80 °C hot water for 1 h. The CCM was then dried in the oven at 80 °C. To prepare the CCMs with different pore-designed anode catalyst layers, different diameters and PSF amounts as the pore forming agent were introduced and labeled as follows:

Without-PSF: Anode catalyst layer without PSF.

1 μm-0.3: Anode catalyst layer containing 30:70 wt ratio of PSF to C of 1-μm PSF.

1 μm-0.5: Anode catalyst layer containing 50:50 wt ratio of PSF to C of 1-μm PSF.

3 μm-0.3: Anode catalyst layer containing 30:70 wt ratio of PSF to C of 3-μm PSF.

3 μm-0.5: Anode catalyst layer containing 50:50 wt ratio of PSF to C of 3-μm PSF.

5 μm-0.3: Anode catalyst layer containing 30:70 wt ratio of PSF to C of 5-μm PSF.

5 μm-0.5: Anode catalyst layer containing 50:50 wt ratio of PSF to C of 5-μm PSF.

2.2. Characterization of pore-designed anode catalyst layer

The morphological images of the pore-designed anode catalyst layers before and after the PSF removal were observed using an SEM. The properties of the pores formed by the PSFs, i.e., the diameter and length, on the pore-designed anode catalyst layers were also measured using an SEM by averaging the information of 50 pores. A micrometer and an SEM were used to measure the thickness, and it was confirmed that there is a slight difference in the thickness of the catalyst layer measured by a micrometer and an SEM. The overall porosity was calculated using the following equation, which was based on the thickness of the catalyst layer and weight loading of the catalyst layer components [28]:

$$\varepsilon = \frac{t_{cl} - t_{compact}}{t_{cl}} \quad \text{Eq.1}$$

where t_{cl} is the thickness of the catalyst layer, [cm], and the $t_{compact}$ was calculated based on the weight loading of the catalyst layer components, [cm], calculated as follows:

$$t_{compact} = \frac{m_N}{\rho_N} + \frac{m_c}{\rho_c} + \frac{m_{Pd}}{\rho_{Pd}} \quad \text{Eq.2}$$

where m_N, m_C, and m_{Pd} are the weight loadings of Nafion, carbon, and palladium, [g/cm^2], respectively. ρ_N, ρ_C and ρ_{Pd} are the densities of the Nafion, carbon and palladium, and are considered to be 2.00, 1.80 and 12.02, [g/cm^3], respectively [28,29].

2.3. Single cell assembly and performance evaluation

The DFAFC single cell (FC-05-02H2R, ElectroChem, Inc.) was assembled by hot-pressing the CCM with untreated carbon cloth (CC plain, Fuel Cell Earth) at 140 °C and 5 MPa for 3 min to form a membrane electrode assembly (MEA). The MEA was then sandwiched between a graphite plate containing serpentine flow channel current collectors and a silicone sheet. Before conducting the performance test of the different MEAs, a single cell pre-treatment was required by performing the current-time (i-t) test for 1 h and subsequently performing the current-voltage (i-V) test. The (i-t) and (i-V) tests were repeated several times until a stable performance was achieved with at least three curves of (i-V)s being completely fitted. The pre-treatment was conducted at the single cell operating temperature of 60 °C, 5 M formic acid concentration and 500 mL/min dry oxygen using an electrochemical measurement system (IT8512C+, ITECH Electronics Co., Ltd.).

To observe the effect of different pore-designed anode catalyst layers containing different PSF diameters and amounts on the DFAFC performance characteristics, the DFAFCs were operated at the two different temperatures of 30 °C and 60 °C using 3 M, 5 M and 7 M formic acid concentrations and 700 mL/min oxygen gas flow rate. During the performance test, the anode performance will be degraded due to catalyst poisoning. Hence, the regeneration process needs to be performed after each power generation by washing the anode surface using deionized water until the cell voltage was reduced to 0.1 V [30,31].

Table 1
The mean diameters and lengths of the PSF and the pores formed in the catalyst layer.

Sample	The mean diameter of PSF used (μm)	The mean length of PSF used (μm)	The mean diameter of pore formed (μm)	The mean length of pore formed (μm)
1 μm-0.3	1.1	16.1	0.9	10.6
1 μm-0.5			0.7	11.7
3 μm-0.3	3.3	23.1	2.2	18.8
3 μm-0.5			2.1	16.9
5 μm-0.3	5.5	19.3	4.3	14.7
5 μm-0.5			4.0	17.6

2.4. CF measurement

The formic acid CF was estimated by measuring the CO_2 concentration at the cathode's outlet [30]. The DFAFC was operated at the constant currents of 0 A and 1 A to observe the formic acid transport characteristics under open and closed circuit conditions. It was also operated under the same operating temperatures and acid concentrations as in the performance test evaluation (Section 2.3). The CO_2 gas was collected using a sampling bag at the cathode's outlet through the cold trap and the concentration of the collected CO_2 gas was then determined by using a gas analyzer (GCT-7100, Shimadzu Corporation). It was assumed that the formic acid permeated from the anode through the electrolyte membrane at the cathode catalyst layer was completely and immediately oxidized to CO_2. Hence, the CO_2 concentration at the cathode's outlet was estimated as the formic acid CF.

3. Results & discussion

3.1. The characteristics of the PSF and the pore-designed anode catalyst layers

The morphological images of the different PSF diameters fabricated by electrospinning are shown in Fig. S1. It was confirmed that long and uniform PSFs were formed with the mean diameters of 1.1 μm, 3.3 μm and 5.5 μm. The morphological images of the shortened PSF are also shown in Fig. S2. It was found that the mean lengths of the shortened PSFs were nearly controlled around 20 μm, i.e., 16.1, 23.1, and 19.3 μm, for the 1-μm, 3-μm, and 5-μm PSF diameters, respectively.

Fig. 1 shows the morphological images of the pore-designed anode catalyst layers after removal of the 0.3 and 0.5 amounts of the 1-μm diameter PSF (Fig. 1 a and b), 3-μm diameter PSF (Fig. 1 c and d) and 5-μm diameter PSF (Fig. 1 e and f). A higher magnification of the morphological images for the 1-μm diameter PSF is also demonstrated in the box in Fig. 1 a and b, for larger observations. Moreover, further morphological images at a higher magnification are shown in Fig. S3 to measure the mean pore diameter and length, which are then summarized in Table 1 along with the used PSF properties. According to the table, it was found that the mean pore diameter formed on the catalyst layers increased as the diameter of the PSF increased, with the 1-μm PSF forming 0.7–0.9 μm, and the 3 and 5-μm PSF forming 2.1–2.2 μm and

Table 2
The characteristics of the pore-designed anode catalyst layers prepared by the different PSF diameters and amounts.

Sample	Catalyst and ionomer loading in catalyst layer		Thickness of catalyst layer (μm)	Overall porosity of catalyst layer (%)
	Pd loading (mg-Pd/cm^2)	Ionomer loading (mg/cm^2)		
Without-PSF	1.29	1.61	57.6	65.9
1 μm-0.3	1.27	1.60	72.5	72.7
1 μm-0.5	1.36	1.70	74.1	71.7
3 μm-0.3	1.28	1.60	62.2	68.5
3 μm-0.5	1.35	1.70	66.7	68.6
5 μm-0.3	1.22	1.53	58.9	68.0
5 μm-0.5	1.40	1.75	63.1	66.5

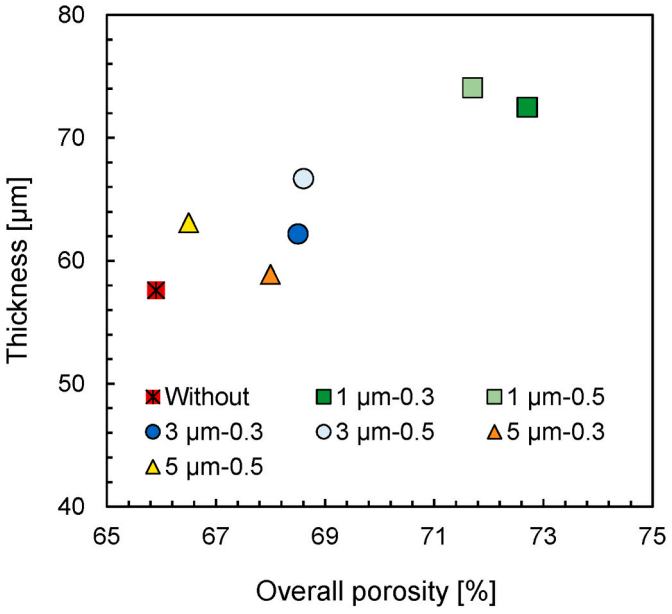

Fig. 2. Correlation between thickness and overall porosity of the different pore-designed anode catalyst layers.

4.3–4.0 μm, respectively. Moreover, all the pore-designed anode catalyst layers have a somewhat similar mean pore length of 10.6–18.8 μm. When comparing the catalyst layer designed from the different pore diameters under the same PSF loading (amount), as shown in Fig. 1 a, c, and e, and Fig. 1 b, d, and f, the number of pores formed by the PSF in the catalyst layers decreased as the diameter of the PSF increased, regardless of the PSF amount (0.3 or 0.5). This result is in accordance with the study conducted by Lee et al. [22] which demonstrated that the pore volume decreased as the diameter of the particle pore former increased. On the other hand, the number of pores increased when increasing the PSF amount from 0.3 to 0.5 (Fig. 1 a to b), (Fig. 1 c to d) and (Fig. 1 e to f). For comparison, there were no additional pores shown in the catalyst layer without-PSF, as seen in Fig. 1 g.

The characteristics of the pore-designed anode catalyst layers are summarized in Table 2. It was found that the catalyst loadings were controlled to be nearly the same with the highest percentage difference being only 13%. However, it was also found that the thickness of the catalyst layers increased with the addition of the PSF compared to that of without the PSF, regardless of the PSF diameters or amounts. For the different PSF diameters, increasing the PSF diameters from 1-μm to 5-μm caused a decrease in the thickness of the catalyst layer regardless of the PSF amounts used. This could be due to a decrease in the number of pores formed by the PSF as the PSF diameter increased, as seen in the morphological images of Fig. 1. On the other hand, the thickness of the catalyst layer increased as the PSF amounts increased from 0.3 to 0.5 for all the PSF diameters, which would be due to an increase in the number of pores in the catalyst layer, as seen in the morphological images of Fig. 1.

In addition, the overall porosity of the catalyst layers shown in Table 2 also increased as the PSFs were added to the catalyst layers as compared to catalyst layer without-PSF, irrespective of the PSF diameters and amounts. We also found that the overall porosity of the catalyst layer decreased with the increasing PSF diameters, regardless of the PSF amounts. This result is consistent with the morphological images shown in Fig. 1 where the number of pores decreased as the PSF diameters increased. On the other hand, the overall porosity slightly changed, or no clear trend was observed when the PSF amount increased from 0.3 to 0.5 for all the PSF diameters. Furthermore, the correlation between the thickness and the overall porosity for the different PSF properties has been further summarized in Fig. 2. It was found that a highly porous structure containing small pores with a thick catalyst layer has been formed by using a smaller PSF diameter, whereas a less porous catalyst layer containing larger pores with a thin catalyst layer was formed by using a larger PSF diameter. Thus, this indicated that the utilization of different PSF diameters and amounts as a pore forming agent exhibited different structures and characteristics of the catalyst layers.

3.2. Effect of pore-designed anode catalyst layer on DFAFC power generation and mass transport characteristics at 30 °C operating temperature

3.2.1. Impact of pore-forming by PSF on the power generation and mass transport characteristics

The power density and polarization curve of the pore-designed anode catalyst layers using different PSF diameters and amounts at a 30 °C operating temperature are shown in Fig. S4. The maximum power density (MPD), limiting current density (LCD) and crossover flux under open circuit (CF–O) and closed circuit (CF–C) conditions are further summarized in Fig. 3 a, b, c and d, respectively. All the parameters, i.e., MPD, LCD, CF-O and CF-C, increased with the increasing formic acid concentration for all the MEAs. These results imply that the improvement of the overpotential due to mass transport in the anode is more significant compared to the increase in the overpotential due to an increase in the CF, irrespective of with or without pore-forming.

Referring to the effect of the pore-forming on the power generation and mass transport in the DFAFC, a higher MPD was obtained when 3-μm and 5-μm PSFs were used as the pore former. Similarly, the LCD, CF-O and CF-C also increased in these cases suggesting that the mass transport in the anode catalyst layer could be improved by selecting the appropriate PSF properties, such as a 3 or 5-μm PSF diameter. A similar (at 0.3) or lower (at 0.5) MPD was observed when a 1-μm PSF was used compared to that of without-PSF. In these cases, LCD and CF-O were also similar at 0.3, and lower at 0.5 compared to that of without-PSF. On the other hand, the 1-μm PSF showed a higher CF-C compared to the case of the without-PSF. This would be related to the thickness of the catalyst layer and the liquid saturation in these catalyst layers. CO_2 is produced by the electrochemical reaction, and it is transported through the anode electrode, which consists of a catalyst layer and diffusion layer, to the channel under the closed circuit condition. On the other hand, there is no production of CO_2 during the open circuit condition. Therefore, the liquid saturation, which is the liquid volume fraction in the open pores in the catalyst layer, decreases under the closed circuit condition. Without-PSF, the CF-C was significantly lower than the CF-O. This is attributed to not only the reduction in the fuel concentration due to the consumption of the fuel by the electrochemical reaction, but also the reduction in the liquid saturation in the anode catalyst layer by the accumulation of the CO_2 produced by the electrochemical reaction. The fact that the increase in the CF, i.e., the improvement of the mass

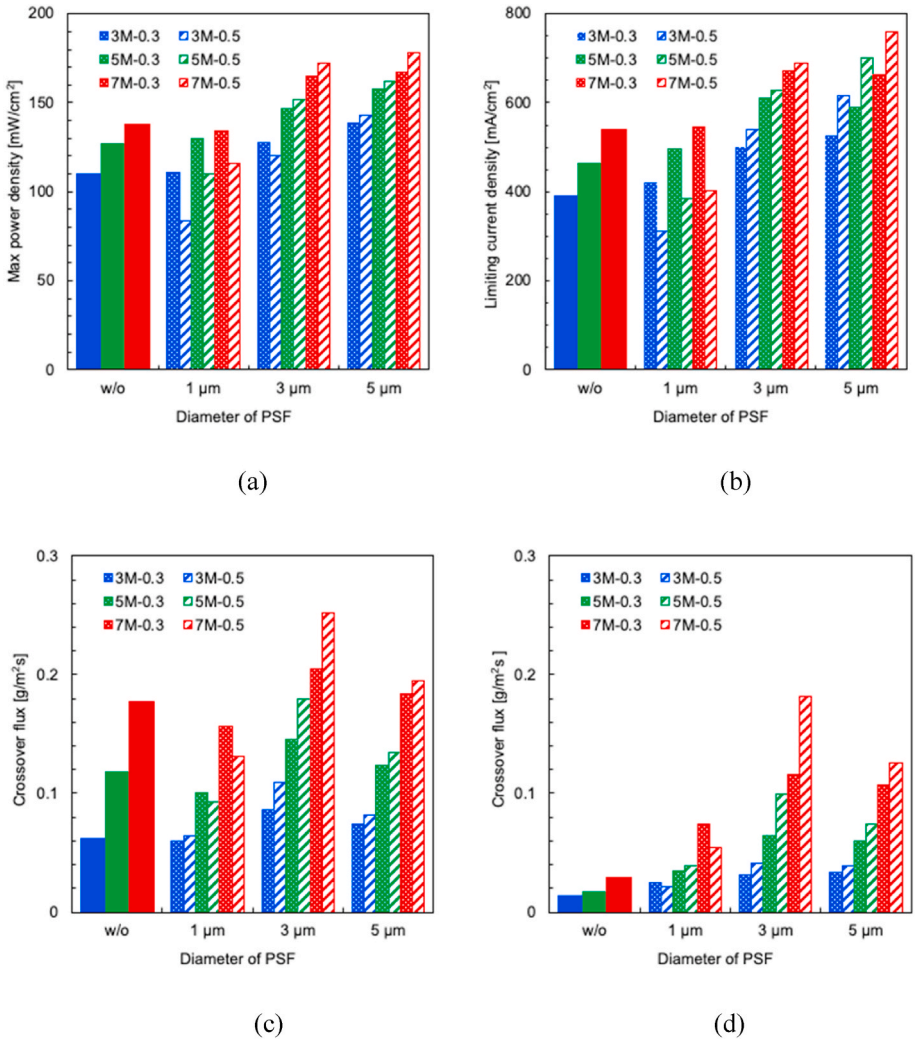

Fig. 3. MPD a), LCD b), CF-O c) and CF-C d) using 3 M, 5 M and 7 M formic acid concentrations at 30 °C of DFAFC operation.

transport in the anode by PSF, is more significant under the closed-circuit condition than under the open-circuit condition, irrespective of the PSF diameters, supports the above consideration. On the other hand, the thickness of the catalyst layer was greater in the case of the 1-μm PSF than the without-PSF. The thick catalyst layer causes an increase in the diffusion distance which causes a significant decrease in the concentration. Due to this result, the concentration of fuel in the anode catalyst layer significantly decreased for the 1-μm PSF and the overpotential of the anode also increased resulting in a lower MPD. Based on this situation, it is considered that the pores made by the appropriate PSF could contribute to preventing the decrease in the liquid saturation caused by the CO_2 removal.

3.2.2. *Effect of PSF diameter on the power generation and mass transport characteristics*

As shown in Fig. 3, the MPD increased with the increasing PSF diameters, irrespective of the PSF amounts (0.3 or 0.5) and formic acid concentrations (3 M–7 M). On the other hand, the CF-O and CF-C were the highest for the 3-μm PSF diameter. This would be related to the capillary force. The capillary force is high for the small pores; hence, the liquid transport improves and the saturation in the catalyst layer increases [32]. Due to this result, CF at 3-μm was higher than that at 5-μm irrespective of the PSF amounts. On the other hand, the MPD of the 5-μm was higher compared to the 3-μm irrespective of the concentration and amount as seen in Fig. 3 a. This is due to a higher CF, which causes a potential drop by the mixed potential at the cathode for a 3-μm PSF. A higher CF also causes an increase in the liquid saturation at the cathode, which causes a potential drop in the cathode, either by the formic acid crossed-over itself or by the generated water from the direct oxidation of the formic acid that crossed-over; thus, the LCD of the 3-μm PSF would be lower than that of the 5-μm PSF one, despite the fact that the 3-μm CF was higher. Considering these situations, a liquid saturation of 1-μm should also be considered high. However, the thickness of the catalyst layer of the 1-μm PSF was much higher compared to the other PSF diameters, resulting in a lower MPD and accompanied by a lower transport rate of the formic acid.

3.2.3. *Effect of PSF amount on the power generation and mass transport characteristics*

Referring to the effect of the PSF amount, it was found that a higher PSF amount (0.5 PSF loading) showed a higher CF and LCD resulting in the higher MPD in the case of the 3-μm and 5-μm PSF diameters. This result suggested that MPD was improved by the improvement of the mass transport due to the increased PSF amount in the anode catalyst layer. However, the thickness of the catalyst layer and porosity shown in Table 2 only slightly varied. Therefore, the increase in the mass transport rate would be considered to be caused by a decrease in the tortuosity of the pores and/or an increase in the amount of the through pores with the increasing PSF amount. This needs to be clarified in a future study.

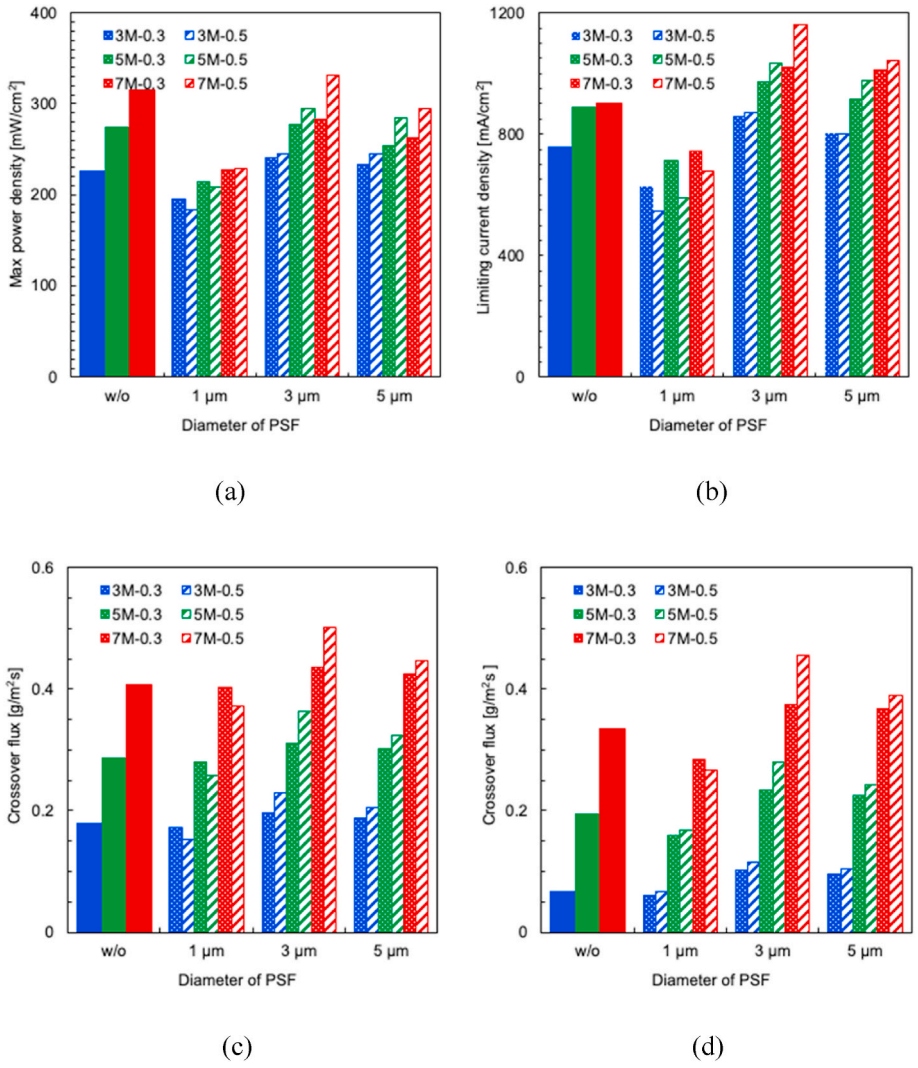

Fig. 4. MPD a), LCD b), CF-O c) and CF-C d) using 3 M, 5 M and 7 M formic acid concentrations at 60 °C of DFAFC operation.

In the 1-μm case, the CF, LCD and MPD decreased with the increasing PSF amount, suggesting that the performance decreased by the poor mass transport in the anode when the PSF amount was increased. Moreover, the thickness and porosity of the catalyst layer shown in Table 2 only slightly varied when the PSF amount increased from 0.3 to 0.5, similar to those of 3 and 5-μm PSFs. As previously stated in Section 3.2.2, the capillary force is high when the pore size is small. In other words, CO_2 was difficult to exhaust to the diffusion layer through the pore-filling liquid since the capillary pressure is low, i.e., the liquid pressure was high. Under such a situation, the accumulation of CO_2 in the pores would be enhanced even though the pore volume, tortuosity and/or amount of the through pores varied. The accumulated CO_2 in the pores blocks the fuel delivery, which causes a decrease in the mass transport and catalyst-fuel contact. Therefore, the performance was not improved when the PSF amount increased for the 1-μm PSF.

3.3. Effect of pore-designed anode catalyst layer on DFAFC power generation and mass transport characteristics at 60 °C operating temperature

The effect of the different diameters and PSF amounts on the DFAFC power generation and mass transport characteristics was further investigated at the operating temperature of 60 °C. The power density and polarization curve are shown in Fig. S5, and its MPD, LCD, CF-O and CF-C are summarized in Fig. 4 a, b, c and d. Based on these figures, a similar trend can be seen as at the low operating temperature as shown in Fig. 3, where the MPD, LCD and CF increased with the increasing concentration of formic acid for all the MEAs. Comparing the LCD and CF between the MEAs with PSF and without the PSF, they increased when the 3-μm and 5-μm PSFs were used. This means that the mass transport rate increased by using the 3-μm and 5-μm PSFs. On the other hand, the MPD was not improved by adding the PSF except for the case of 3 μm-0.5 ones. In these situations, the effect of the improvement of the mass transport at the anode would be less significant compared to the performance decrease in the cathode due to the higher CF. However, in the case of the 3 μm-0.5, the mass transport rate and liquid saturation significantly increased, as mentioned in Section 3.2 compared to the other cases, resulting in the highest MPD of 331 mw/cm^2 with a 5% increment compared to without- PSF. Moreover, the 1-μm PSF diameter showed the lowest MPD with a lower or similar LCD, irrespective of the PSF amounts, similar to that at the low operating temperature, generally due to a lower mass transport rate when compared to the other MEAs.

Interestingly, it was noted that in Fig. 4 d, the without-PSF showed a higher CF-C at 60 °C when compared to the 1-μm PSF. However, the CF of the without-PSF was lower at the low operating temperature of 30 °C as seen in Fig. 3 d. This would be due to the higher vapor pressure as the cell operating temperature was increased. Since increasing the cell operating temperature raises the fuel vapor pressure [33,34], and the vapor-phase transport is greater than the liquid-phase during the low liquid saturation (closed circuit condition) [35]. Therefore, due to this

Table 3
Comparison findings using various pore formers in the anode catalyst layer of DLFC.

References	Type of Fuel Cell	Pore former	Properties of pore former	Cell operating temperature, [°C]	Max. power density, [mW/cm^2]	Percentage performance improvement, [%]	Analysis related to mass transport study
[19]	DMFC	Li_2CO_3 particle	Amount: 0 and 50%	65	120	33	–
[20]	DMFC	NH_4HCO_3 particle	Dual layer: inner layer less porous than outer layer	30	45	40	–
[21]	DFAFC	Li_2CO_3 particle	Amount: 0, 17.5 and 50%	40	114 (17.5%)	21	–
[22]	DMFC	SiO_2 particle	Diameter: 0, 18, 42 and 500 nm	60	125 (500 nm)	89	–
[23]	DMFC	MgO particle	Combination of porous anode and MPL	25	43.7	45	–
This study	DFAFC	Polystyrene fiber (PSF)	Diameter: 0, 1, 3 and 5 μm Amount: 30 and 50%	30 and 60	172 and 331 (3 μm-50%)	25 and 5	Formic acid crossover flux

reason, and the lower thickness of the without-PSF than that of the 1-μm PSF one, the CF of the without-PSF was higher at the 60 °C operating temperature under the closed circuit condition. On the other hand, the CF of the without-PSF decreased at the low operating temperature of 30 °C caused by the lower vapor pressure (liquid phase). Based on this, it was suggested that increasing the cell operating temperature could reduce the capillary force, which is equal to the capillary rise of a liquid level, thereby improving fuel transport by reducing the two-phase flow caused by the higher fuel vapor pressure. This finding is consistent with Jung et al. [35], showing the effect of fuel transport due to the capillary force being higher at a low operating temperature while it is reduced as the cell operating temperature increased.

Referring to the effect of the PSF diameter on the power generation and mass transport characteristics, the MPD, LCD and CF were the highest for the 3-μm PSF diameter among all the cases (MEAs), although the MPD of the 5-μm PSF was the highest among all the MEAs at a low cell temperature, as shown in Fig. 3 a. As previously mentioned, liquid saturation was lower at the higher temperature, hence the liquid transport and/or the saturation due to the capillary action become more significant at the higher cell temperature. Moreover, the improvement in the overpotential caused by the higher mass transport in the anode is more influential than the increase in the cathode overpotential due to the higher CF; thus, the MPD of the 3-μm one was higher following a higher CF at the higher temperature.

Referring to the different PSF amounts on the CF, it shows a similar behavior as at the low operating temperature in which the CF increased as the PSF amount increased for the 3-μm and 5-μm PSFs. On the other hand, the CF was reduced for the 1-μm PSF. This is due to the small diameter of the pores which had a significant impact on increasing the capillary pressure difference for the CO_2 removal, thus lowering the CF and resulting in a lower performance. Based on these results, it is suggested that the 3 μm-0.5 PSF is the appropriate PSF properties for the higher mass transport rate with the higher performance compared to that of the without-PSF at the high operating temperature of 60 °C.

3.4. Comparison of the impact of pore-forming on the power generation characteristics in DLFC with the other related studies

Table 3 shows a comparison of the performance improvement by the pore formers and characteristics of pore formers, i.e., shape, diameter, and amount, in the anode catalyst layer for DLFC reported in the literature with the present study. From the previous studies, a significant improvement in the cell performance were shown as the particle pore formers were added to the anode catalyst layer, regardless of the pore former diameter and amount or cell operating condition. The improvement of the cell performance was discussed due to the higher catalyst utilization caused by higher mass transport with higher catalyst layer porosity. Comparing to the previous study, we have successfully formed a PSF pore former with various diameters using electrospinning, and the maximum power density was the highest compared to the previous studies, even though the percentage of the performance improvement showed a modest increase. Considering the fact that the properties of PSF such as the length and diameter can be easily controlled, the PSF is a promising pore former that can enhance the cell performance with enhancing the mass transport in the anode catalyst layer. However, the effect of the pore former shape, such as the fiber length and aspect ratio, etc., on mass transport and cell performance should be discussed to improve the performance more. Moreover, a numerical simulation will be also needed to visualize the mass transport, such as a distribution of the liquid saturation and vapor pressure since they will significantly affect to the DFAFC performance. Hence, these will be reported in near future.

4. Conclusions

The utilization of different PSF properties (diameter and amount) as pore formers, which were fabricated by electrospinning, has formed different characteristics of the anode catalyst layers. The increase in PSF diameter caused a decrease in the number of pores formed in the catalyst layer and the thickness of the catalyst layer. The results found that the appropriate PSF properties (3 μm-0.5) achieved the highest CF at the operating temperatures of both 30 °C and 60 °C, which improved the MPD by 25% from 138 mW/cm^2 to 172 mW/cm^2 and by 5% from 316 mW/cm^2 to 331 mW/cm^2, respectively, in comparison to the without-PSF. It was due to the characteristics of the catalyst layer having an appropriate pore diameter and catalyst layer thickness, which became a crucial factor for the higher fuel transport and CO_2 removal. It was also suggested that the capillary factor became significant as the operating temperature increased, which enhanced the fuel transport by reducing the two-phase flow caused by the higher fuel vapor pressure, resulting in a higher CF as well as a higher MPD. Thus, this work demonstrated that a pore-designed anode catalyst layer formed by PSF that was fabricated by electrospinning is a promising technique that can be a great incentive for further research on pore-forming structure for higher cell performance caused by higher mass transport.

CRediT authorship contribution statement

Madihah Miskan: Writing – original draft. **Mototake Furuhashi:** Supervision. **Yugo Osaka:** Supervision. **Akio Kodama:** Supervision. **Takuya Tsujiguchi:** Supervision, Writing – review & editing.

Declaration of competing interest

The authors declare that they have no known competing financial interests or personal relationships that could have appeared to influence the work reported in this paper.

Data availability

No data was used for the research described in the article.

Acknowledgement

This study was supported by KAKENHI 22H01858, 21H02037 and New Energy and Industrial Technology Development Organization (NEDO) JPNP20004.

Appendix A. Supplementary data

Supplementary data to this article can be found online at https://doi.org/10.1016/j.jpowsour.2023.232911.

References

[1] B.C. Ong, S.K. Kamarudin, S. Basri, Direct liquid fuel cells: a review, Int. J. Hydrogen Energy 42 (2017) 10142–10157, https://doi.org/10.1016/j.ijhydene.2017.01.117.
[2] C.M. Miesse, W.S. Jung, K.J. Jeong, J.K. Lee, J. Lee, J. Han, S.P. Yoon, S.W. Nam, T. H. Lim, S.A. Hong, Direct formic acid fuel cell portable power system for the operation of a laptop computer, J. Power Sources 162 (2006) 532–540, https://doi.org/10.1016/j.jpowsour.2006.07.013.
[3] K.J. Jeong, C.M. Miesse, J.H. Choi, J. Lee, J. Han, S.P. Yoon, S.W. Nam, T.H. Lim, T. G. Lee, Fuel crossover in direct formic acid fuel cells, J. Power Sources 168 (2007) 119–125, https://doi.org/10.1016/j.jpowsour.2007.02.062.
[4] Y. Zhu, S.Y. Ha, R.I. Masel, High power density direct formic acid fuel cells, J. Power Sources 130 (2004) 8–14, https://doi.org/10.1016/j.jpowsour.2003.11.051.
[5] C. Rice, S. Ha, R.I. Masel, P. Waszczuk, A. Wieckowski, T. Barnard, Direct Formic Acid Fuel Cells, (n.d).
[6] S.Z. Rejal, M.S. Masdar, S.K. Kamarudin, A parametric study of the direct formic acid fuel cell (DFAFC) performance and fuel crossover, Int. J. Hydrogen Energy 39 (2014) 10267–10274, https://doi.org/10.1016/j.ijhydene.2014.04.149.
[7] T. Bewer, T. Beckmann, H. Dohle, J. Mergel, D. Stolten, Novel method for investigation of two-phase flow in liquid feed direct methanol fuel cells using an aqueous H2O2 solution, J. Power Sources 125 (2004) 1–9, https://doi.org/10.1016/S0378-7753(03)00824-3.
[8] H. Yang, T.S. Zhao, Q. Ye, In situ visualization study of CO2 gas bubble behavior in DMFC anode flow fields, J. Power Sources 139 (2005) 79–90, https://doi.org/10.1016/j.jpowsour.2004.05.033.
[9] H.A. Wolf Vielstich, Arnold Lamm, Hubert A. Gasteiger, Harumi Yokokawa, Handbook of Fuel Cells : Fundamentals, Technology, and Applications, Wiley, 2003.
[10] G.Q. Lu, C.Y. Wang, Electrochemical and flow characterization of a direct methanol fuel cell, J. Power Sources 134 (2004) 33–40, https://doi.org/10.1016/j.jpowsour.2004.01.055.
[11] A. Sajid, E. Pervaiz, H. Ali, T. Noor, M.M. Baig, A perspective on development of fuel cell materials: electrodes and electrolyte, Int. J. Energy Res. 46 (2022) 6953–6988, https://doi.org/10.1002/er.7635.
[12] F.M. Souza, V.S. Pinheiro, T.C. Gentil, L.E.B. Lucchetti, J.C.M. Silva, M.L.M. G. Santos, I. de Oliveira, W.M.C. Dourado, G. Amaral-Labat, S. Okamoto, M. C. Santos, Alkaline direct liquid fuel cells: advances, challenges and perspectives, J. Electroanal. Chem. 922 (2022), https://doi.org/10.1016/j.jelechem.2022.116712.
[13] X.Q. Hu, Q.W. Yang, G. Xiao, X.T. Chen, X. Qiu, Power generation enhancement in direct methanol fuel cells using non-uniform cross-sectional serpentine channels, Energy Convers. Manag. 188 (2019) 438–446, https://doi.org/10.1016/j.enconman.2019.03.058.
[14] S.S. Hsieh, H.C. Wu, B.S. Her, A novel design for a flow field configuration, of a direct methanol fuel cell, J. Power Sources 195 (2010) 3224–3230, https://doi.org/10.1016/j.jpowsour.2009.11.119.
[15] Y. Wang, L. Zheng, G. Han, L. Lu, M. Wang, J. Li, X. Wang, A novel multi-porous and hydrophilic anode diffusion layer for DMFC, Int. J. Hydrogen Energy 39 (2014) 19132–19139, https://doi.org/10.1016/j.ijhydene.2014.08.098.
[16] Q.Z. Shu, Z.X. Xia, W. Wei, X.L. Xu, S.L. Wang, H. Zhao, G.Q. Sun, A novel gas diffusion layer and its application to direct methanol fuel cells, Xinxing Tan Cailiao/New Carbon Mater. 36 (2021) 409–419, https://doi.org/10.1016/S1872-5805(21)60017-3.
[17] A. Alrashidi, H. Liu, Laser-perforated anode gas diffusion layers for direct methanol fuel cells, Int. J. Hydrogen Energy 46 (2021) 17886–17896, https://doi.org/10.1016/j.ijhydene.2021.02.199.
[18] Z. Xia, X. Zhang, H. Sun, S. Wang, G. Sun, Recent advances in multi-scale design and construction of materials for direct methanol fuel cells, Nano Energy 65 (2019), https://doi.org/10.1016/j.nanoen.2019.104048.
[19] M.C. Tucker, M. Odgaard, P.B. Lund, S. Yde-Andersen, J.O. Thomas, The pore structure of direct methanol fuel cell electrodes, J. Electrochem. Soc. 152 (2005) A1844, https://doi.org/10.1149/1.1993488.
[20] P. Liu, G.P. Yin, C.Y. Du, Composite anode catalyst layer for direct methanol fuel cell, Electrochem. Commun. 10 (2008) 1471–1473, https://doi.org/10.1016/j.elecom.2008.07.030.
[21] A.S. Bauskar, C.A. Rice, Impact of anode catalyst layer porosity on the performance of a direct formic acid fuel cell, Electrochim. Acta 62 (2012) 36–41, https://doi.org/10.1016/j.electacta.2011.11.057.
[22] Y. Lee, T.K. Kim, Y.S. Choi, Effect of porosity in catalyst layers on direct methanol fuel cell performances, Fuel Cell. 13 (2013) 173–180, https://doi.org/10.1002/fuce.201200014.
[23] Q. Huang, J. Jiang, J. Chai, T. Yuan, H. Zhang, Z. Zou, X. Zhang, H. Yang, Construction of porous anode by sacrificial template for a passive direct methanol fuel cell, J. Power Sources 262 (2014) 213–218, https://doi.org/10.1016/j.jpowsour.2014.03.121.
[24] S. Cavaliere, S. Subianto, I. Savych, D.J. Jones, J. Rozière, Electrospinning: designed architectures for energy conversion and storage devices, Energy Environ. Sci. 4 (2011) 4761–4785, https://doi.org/10.1039/c1ee02201f.
[25] A. Zlotorowicz, K. Jayasayee, P.I. Dahl, M.S. Thomassen, S. Kjelstrup, Tailored porosities of the cathode layer for improved polymer electrolyte fuel cell performance, J. Power Sources 287 (2015) 472–477, https://doi.org/10.1016/j.jpowsour.2015.04.079.
[26] T. Uyar, F. Besenbacher, Electrospinning of uniform polystyrene fibers: the effect of solvent conductivity, Polymer (Guildf). 49 (2008) 5336–5343, https://doi.org/10.1016/j.polymer.2008.09.025.
[27] S. Huan, G. Liu, G. Han, W. Cheng, Z. Fu, Q. Wu, Q. Wang, Effect of experimental parameters on morphological, mechanical and hydrophobic properties of electrospun polystyrene fibers, Materials 8 (2015) 2718–2734, https://doi.org/10.3390/ma8052718.
[28] T. Suzuki, H. Tanaka, M. Hayase, S. Tsushima, S. Hirai, Investigation of porous structure formation of catalyst layers for proton exchange membrane fuel cells and their effect on cell performance, Int. J. Hydrogen Energy 41 (2016) 20326–20335, https://doi.org/10.1016/j.ijhydene.2016.09.078.
[29] B. Sarac, T. Karazehir, E. Yüce, M. Mühlbacher, A.S. Sarac, J. Eckert, Porosity and thickness effect of Pd–Cu–Si metallic glasses on electrocatalytic hydrogen production and storage, Mater. Des. 210 (2021), https://doi.org/10.1016/j.matdes.2021.110099.
[30] T. Tsujiguchi, F. Matsuoka, Y. Hokari, Y. Osaka, A. Kodama, Overpotential analysis of the direct formic acid fuel cell, Electrochim. Acta 197 (2016) 32–38, https://doi.org/10.1016/j.electacta.2016.03.062.
[31] F. Abd Lah Halim, T. Tsujiguchi, Y. Osaka, A. Kodama, Performance of direct formic acid fuel cell using transition metal-nitrogen-doped carbon nanotubes as cathode catalysts, Int. J. Energy Res. 43 (2019) 8070–8084, https://doi.org/10.1002/er.4802.
[32] A. Faghri, Y. Zhang, SOLID-LIQUID-VAPOR phenomena and interfacial heat and mass transfer, in: Transport Phenomena in Multiphase Systems, Elsevier, 2006, pp. 331–420, https://doi.org/10.1016/b978-0-12-370610-2.50010-6.
[33] Z. Guo, A. Faghri, Vapor feed direct methanol fuel cells with passive thermal-fluids management system, J. Power Sources 167 (2007) 378–390, https://doi.org/10.1016/j.jpowsour.2007.02.024.
[34] W. Yuan, B. Zhou, J. Deng, Y. Tang, Z. Zhang, Z. Li, Overview on the developments of vapor-feed direct methanol fuel cells, Int. J. Hydrogen Energy 39 (2014) 6689–6704, https://doi.org/10.1016/j.ijhydene.2014.02.002.
[35] S. Jung, Y. Leng, C.Y. Wang, Role of co2 in methanol and water transport in direct methanol fuel cells, Electrochim. Acta 134 (2014) 35–48, https://doi.org/10.1016/j.electacta.2014.04.087.